

Multiscale Vision Transformers meet Bipartite Matching for efficient single-stage Action Localization

Ioanna Ntinou^{†,1} Enrique Sanchez^{†,2} Georgios Tzimiropoulos^{1,2}
¹Queen Mary University London, UK ²Samsung AI Center Cambridge, UK

[†]Equal contribution

i.ntinou@qmul.ac.uk kike.sanc@gmail.com g.tzimiropoulos@qmul.ac.uk

Abstract

Action Localization is a challenging problem that combines detection and recognition tasks, which are often addressed separately. State-of-the-art methods rely on off-the-shelf bounding box detections pre-computed at high resolution and propose transformer models that focus on the classification task alone. Such two-stage solutions are prohibitive for real-time deployment. On the other hand, single-stage methods target both tasks by devoting part of the network (generally the backbone) to sharing the majority of the workload, compromising performance for speed. These methods build on adding a DETR head with learnable queries that, after cross- and self-attention can be sent to corresponding MLPs for detecting a person’s bounding box and action. However, DETR-like architectures are challenging to train and can incur in big complexity.

In this paper, we observe that **a straight bipartite matching loss can be applied to the output tokens of a vision transformer**. This results in a backbone + MLP architecture that can do both tasks without the need of an extra encoder-decoder head and learnable queries. We show that a single MViT-S architecture trained with bipartite matching to perform both tasks surpasses the same MViT-S when trained with RoI align on pre-computed bounding boxes. With a careful design of token pooling and the proposed training pipeline, our MViT2-S model achieves +3 mAP on AVA2.2. w.r.t. the two-stage counterpart. Code and models will be released after paper revision.

1. Introduction

Action Localization is a challenging task that requires detecting a person’s bounding box within a given frame and classifying their corresponding actions. This task shares similarities with object detection, with the particularity that the detected objects are always people and the classes correspond to various actions that can sometimes co-occur. It

poses the additional challenge that actions require temporal reasoning, as well as the fact that a person detector can contribute to false positives if a given person is not performing any of the target actions. The current golden benchmark of AVA 2.2. [17] has a fairly low mean Average Precision (mAP) compared to that of e.g. COCO [22].

Interestingly, state-of-the-art approaches achieving high absolute absolute mAP outsource the detection task to a pre-trained Faster-RCNN [27], and focus on large capacity networks and the use of large pre-training data (see Fig. 1a)). These methods serve the purpose of boosting the absolute performance by means of accuracy but are in many cases prohibitive even for standard GPU accelerators.

In this paper, we contribute to the domain of low-regime scalable models that perform both the detection and the recognition tasks. Because of its similarities with the object detection task, many recent methods targeting a single-stage model build on having a strong backbone that provides temporal features to a DETR [1] architecture [41, 43]. A DETR architecture is an encoder-decoder transformer with learnable queries that are assigned to the ground-truth pairs of bounding box/action in a set prediction fashion (Fig. 1b)).

While DETR-based architectures have shown to be efficient choices for end-to-end action localization (i.e. for joint detection and classification tasks), their design involves a video backbone and an encoder-decoder transformer architecture. This poses the question of whether there is room for further improvement in the network design. To answer this question, we draw inspiration from the recent advances in Open-World Object Detection using Vision Transformers (OWL-ViT [24]) and make the following **contribution**: we propose the use of a bipartite matching loss between the spatio-temporal output embeddings of a single transformer backbone and the ground-truth instances in a video clip (Fig. 1c). In this setting, the video embeddings are independent tokens that can be matched to the predictions similarly to that of DETR. This implies that a) no learnable tokens are necessary, nor a transformer decoder with self- and cross-attention, and b) the video backbone and the encoder can

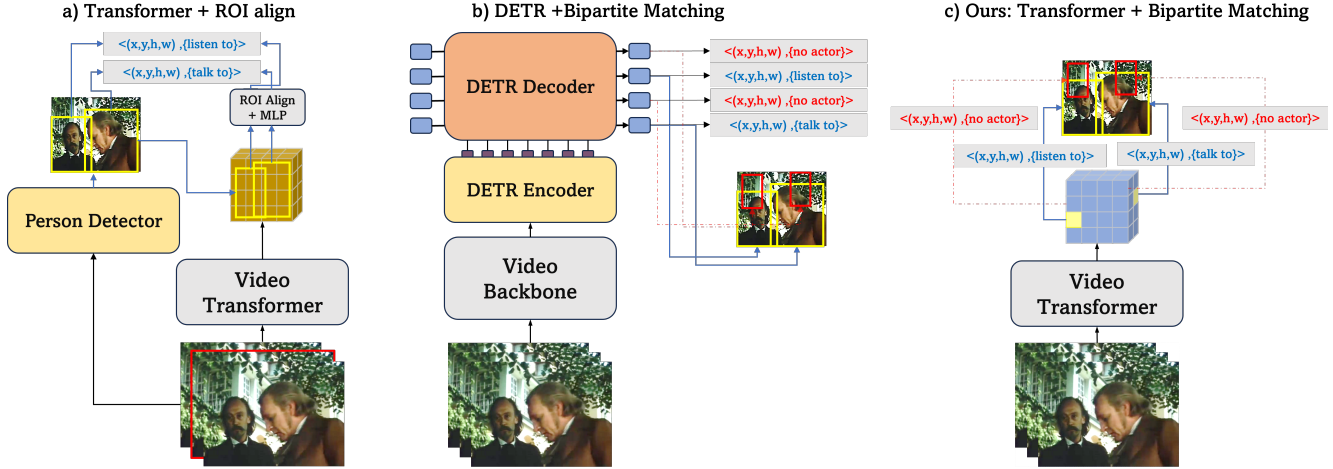


Figure 1. Comparison between existing works and our proposed approach. **a)** Traditional two-stage methods work on developing strong vision transformers, that are applied in the domain of Action Localization by outsourcing the bounding box detections to an external detector. ROI Align is applied to the output of the transformer using the detected bounding boxes, and the pooled features are forwarded to an MLP that returns the class predictions. **b)** Recent approaches in one-stage Action Localization leverage on the DETR capacity to model both the bounding boxes and the action classes. A video backbone produces strong spatio-temporal features that are handled by a DETR transformer encoder. A set of learnable queries are then used by a DETR transformer decoder to produce the final outputs. **c)** **Our method** builds a vision transformer only that is trained against a bipartite matching loss between the individual predictions given by the output spatio-temporal tokens and the ground-truth bounding boxes and classes. Our method does not need learnable queries, as well as a DETR decoder, and can combine the backbone and the DETR encoder into a single architecture.

be merged into a single strong video transformer. Such a simple approach with a careful token selection allows us to train an MVITv2-S [19] with a simple MLP head to directly predict the bounding boxes and the action classes. Without additional elements or data, our single-stage MVITv2-S surpasses the two-stage MVITv2-S of [19] that was trained using RoI align and pre-computed bounding boxes.

Our main results indicate that with similar FLOPs an MVITv2-S trained with bipartite matching performs better than the same MVITv2-S when trained only for action classification from precomputed bounding boxes. In addition, by simply removing the last pooling layer of MVITv2-S we obtain a +3 mAP increase on AVA2.2 [17]. To the best of our knowledge, our method is the first to apply an encoder-only vision transformer for action localization with a bipartite matching loss.

2. Related Work

Two-stage spatio-temporal action localization: Most existing works on action detection [5, 6, 25, 33, 36, 38–40, 42] depend on a supplementary person detector for actor localization. Typically that is a Faster RCNN-R101-FPN [27] detector, originally trained for object detection on COCO [20] dataset and subsequently fine-tuned on the AVA [9], is incorporated in the action detection task. By introducing an off-the-self detector, the action detection task is simplified to an action classification problem. For actor-specific prediction, the RoIAlign [11] operation is applied to the generated

3D feature maps. The aforementioned standard pipeline is employed by SlowFast [6], MVIT [19], VideoMAE [35] and Hiera [29] where RoI features are directly utilized for action classification. However, such features only confine information within the bounding box, neglecting any contextual information beyond it. To address the limitation, AIA [34] and ACARN [25] employ an additional heavyweight module to capture the interaction between the actor and the context or other actors. Furthermore, to model temporal interactions, MeMVIT [39], incorporated a memory mechanism on an MVIT [19] backbone. While achieving high accuracy, these methods are inefficient for real-world deployment. Our method is on par with the state-of-the-art MeMVIT requiring fewer FLOPs.

Single-stage spatio-temporal action localization: Motivated by the aforementioned limitation of the traditional two-stage pipeline for action detection and classification, several works attempted to tackle both detection and classification in a unified framework. Some works borrow solutions developed for object detection and adapt them to action detection [41, 43] while others simplify training through joint actor proposal and action classification networks [3, 8, 15, 32, 33]. SE-STAD [32] builds on the Faster-RCNN framework of [27] and incorporates into it the action classification task. Similarly, the Video action transformer network [8] is a transformer-style action detector to aggregate the spatio-temporal context around the target actors. More recent works [2, 41, 43] leverage on recent advancements of DETR in object detection, and hence, they propose

to form the task using learnable queries to model both action and bounding boxes. TubeR [43] proposed a DETR-based architecture where a set of queries, coined Tubelet Queries, simultaneously encode the temporal dynamics of a specific actor’s bounding box as well as their corresponding actions. TubeR uses a single DETR head to model the Tubelet Queries, with a classification head that requires an extra decoder for the queries to attend again to the video features. In a similar fashion, DETR-like fashion, STMixer [41] proposes to adaptively sample discriminative features from a multi-scale spatio-temporal feature space and decode them using an adaptive scheme under the guidance of queries. EVAD [2] suggests two video action detection designs: 1) Token dropout focusing on keyframe-centric spatiotemporal preservation and 2) Scene context refinement using ROI align operation and a decoder. Contrary to previous works that use a decoder or a heavy module that introduces interaction features of context or other actors, we demonstrate that a single transformer model trained directly with a bipartite matching can achieve similar accuracy to more complex solutions based on DETR.

3. Method

To motivate our approach, we first depart from a standard application of Vision Transformers for Action Localization with pre-computed bounding boxes, to then provide a brief description of single-stage methods that build on using bipartite matching (i.e. DETR). We then introduce our approach: a Video Transformer with bipartite matching, without learnable queries and decoder.

3.1. Problem definition

The goal of Action Localization is to detect and classify a set of actions in the central frame I_t of a video clip X composed of T frames. Because not every person in a video clip might be performing an action of interest, we distinguish between a person and an *actor*, i.e. a person doing any of the C target *actions*. An actor at time t is defined by a *bounding box* $\mathbf{b} = [x_c, y_c, h, w]$, with x_c, y_c the normalized coordinates of the box center and h, w the normalized height and width of the box, and an *action class* one-hot vector $\mathbf{a} = \{0, 1\}^C$ representing the activation or not of each class. The action classes do not need to be mutually exclusive (e.g. “talk to” and “listen” can co-occur).

3.2. Vision Transformers for Action Localization

Multi-scale Vision Transformers (MViT, [4, 19]) are self-attention-based architectures that operate on *visual tokens* produced by dividing the input video (or image) into $\tilde{L} = T \times H \times W$ patches of size $3 \times (\tau\nu\nu)$, and by projecting each into D -dimensional embeddings through a linear or a convolutional layer. MViT architectures operate hierarchically considering many small input patches of few channels

D , progressively increasing the patch size and the channel dimensions through pooling layers. Without loss of generality, we define a (Multi-scale) Vision Transformer as a network \mathcal{V} that produces an output set of \tilde{L} tokens of d dimensions from an input clip $X \in \mathbb{R}^{D \times T \times H \times W}$, as $\tilde{X} = \mathcal{V}(X) \in \mathbb{R}^{\tilde{L} \times d}$, with $\tilde{L} = t \times h \times w$, and $t \leq T, w \leq W, h \leq H$.

Generally, Vision Transformers are first pre-trained on Action Recognition datasets with video-only mutually exclusive classes, using an additional class token X_0 prepended to X . Then, Vision Transformers are adapted to Action Localization tasks by using an *external* actor detector (i.e. a person detector fine-tuned to return positives on actors only) that provides a bounding box $\hat{\mathbf{b}}$. The output \tilde{L} is then treated as a spatio-temporal feature map: ROI-align is done on the temporally pooled feature map $h \times w$ using $\hat{\mathbf{b}}$, and forwarded to an action classifier to produce the action class probabilities $p(\hat{\mathbf{a}})$.

These models, known as *two-stage*, compromise complexity for accuracy, resulting in solutions with prohibitive complexity. Existing works use a state-of-the-art Faster-RCNN detector to compute the bounding boxes, resulting in models with added complexity of 246 GFLOPs, regardless of the size of the proposed architectures. While MViT has recently been proposed for object detection by adding Mask-RCNN [11] and Feature Pyramid Networks [21], the use of a single architecture to perform both detection and action classification is unexplored. Nonetheless, to the best of our knowledge, ours is the first Vision Transformer that can do bounding box detection and action classification in a single step.

3.3. DETR for Action Localization

DETR (DEtection TRansformers [1]) formulate object detection as a bipartite matching problem where a fixed set of L learnable embeddings, known as object queries, are one-to-one matched to a list of predictions of the form $\langle \mathbf{b}, p(\hat{\mathbf{a}}) \rangle$, with $\hat{\mathbf{a}}' = \{\hat{\mathbf{a}}, \emptyset\}$ the list of C target classes (objects in this case) appended with the empty class \emptyset representing a no-object class. During training, the Hungarian Algorithm [16] is used to map the $N < L$ objects in an image to the “closest” predictions so that the assignments minimize a combined bounding box and class cost. The $L - N$ remaining predictions are assigned to the empty class. The learning is done by backpropagating the bounding box and class error for those outputs matched to a ground-truth object, and only the class error for those assigned to the empty class (i.e. to enforce bounding boxes that do not correspond to an object to be tagged as \emptyset).

DETR possesses appealing properties for Action Localization, as the learnable object queries can convey object localization and action classification. The handful of proposed approaches that have ventured to apply DETR to Action Localization are faithful to the DETR configuration [41, 43]:

a 3D backbone produces video features that are fed into a transformer encoder to produce a hierarchy of features, and a transformer decoder transforms the learnable queries through self- and cross-attention layers between the queries and the encoder features, producing a fixed set of L outputs. However, rather than appending the target classes with the empty class, a dedicated *actor detector* head is used to determine if a bounding box corresponds to an actor or not. The outputs are now triplets of the form $\langle \mathbf{b}, p(\alpha), p(\hat{\mathbf{a}}) \rangle$, with $p(\alpha)$ being a two-logit vector representing the actor and the \emptyset classes. The use of a DETR encoder-decoder architecture offers a good tradeoff between accuracy and complexity with the decoder alleviating part of the backbone’s complexity. However, these approaches still suffer from a complex architecture and a limited number of queries that can be used to train the models.

3.4. Our solution

Herein, we observe that neither the backbone nor the decoder are necessary to achieve a good accuracy-speed tradeoff, and we follow the recent advances in Open-Vocabulary Object Detection (OWL-ViT [24]) to motivate our approach. OWL-ViT introduces a CLIP vision transformer encoder with the last pooling layer removed. Instead of pooling the output tokens to form a visual embedding to be mapped into the text embeddings as in the standard CLIP image-text matching, each of the output embeddings is forwarded to a small head consisting of a bounding box MLP and a class linear projection. This way, the $\tilde{L} = h \times w$ output tokens from the vision encoder are treated as independent output pairs $\langle \hat{\mathbf{b}}, p(\hat{\mathbf{a}}) \rangle$. These pairs are matched to the ground truth using DETR’s bipartite matching loss. In OWL-ViT, the image patches play the role of the object queries.

To adapt OWL-ViT to the domain of Action Localization, we first note that Multi-scale Vision Transformers are a natural pool of spatio-temporal output embeddings that can be one-to-one matched to triplets $\langle \hat{\mathbf{b}}, p(\alpha), p(\hat{\mathbf{a}}) \rangle$. As we demonstrate in §5.1, a simple MViTv2 architecture trained with bipartite matching achieves higher accuracy than the same MViTv2 trained for Action Localization using external bounding boxes. Notably, our approach does not add additional complexity to the backbone, given that the heads are simple MLPs.

The output of the video transformer, as introduced in §3.2, is $\tilde{X} = \mathcal{V}(X) \in \mathbb{R}^{\tilde{L} \times \tilde{D}}$, with $\tilde{L} = t \times h \times w$ corresponding to the output sequence length. For an input video of $16 \times 256 \times 256$, an MViT produces an output of $8 \times 8 \times 8$ tokens, i.e. $\tilde{L} = 512$, which outnumbers DETR-based architectures. The number of output tokens does not affect the complexity of the network as these are independently processed by three MLPs. Following OWL-ViT, we add a bias to the predicted bounding boxes to make each be centered by default on the image patch that corresponds to the 2D grid in which the

output tokens would be re-arranged. As reported in [24], “there is no strict correspondence between image patches and tokens representations”; however, “biasing box predictions speeds up training and improves final performance”. In our 3D space-time setting, we add the same 2D bias to all tokens on the same 2D grid along the temporal axis.

While tokens are assigned independently, these are obviously position-dependent due to the relative position embeddings that are considered according to their position in a video. The tasks of actor detection and action classification are opposed by definition: actors are to be localized at the central frame, and actions do benefit from the temporal support. Also, it is known that object detection benefits from larger output sizes (cf. Table 1 in [24] uses a resolution of 768 px). To avoid poor detection, we remove the last pooling layer of the MViTv2 architecture, which suffices to produce an output of $\tilde{L} = 8 \times 16 \times 16 = 2048$ tokens, and study how these can be pooled to form the final list of predictions. We note that the main technical limitation resides in that the actor tokens (i.e. those used to regress the bounding boxes and the actors’ likelihood) must be in one-to-one correspondence with the action tokens (i.e. those used to predict the class logits). Bearing this in mind, we choose to use the $\tilde{L} = 512$ tokens corresponding to the two central frames (i.e. $t = 3$ and $t = 4$), to produce $\hat{\mathbf{a}}$ and $p(\alpha)$. To produce the action tokens, we apply temporal pooling on the past and future tokens w.r.t. the central frame independently, i.e. we compute $\tilde{X}'_{t < T/2} \in \mathbb{R}^{h \times w}$ and $\tilde{X}'_{t > T/2} \in \mathbb{R}^{h \times w}$ as

$$\tilde{X}'_{i,j} = (2/t) \sum_{t' < T/2} \tilde{X}_{t',i,j} \text{ for } i, j \in [1 \dots h, 1 \dots w], \quad (1)$$

and

$$\tilde{X}'_{i,j} = (2/t) \sum_{t' > T/2} \tilde{X}_{t',i,j} \text{ for } i, j \in [1 \dots h, 1 \dots w], \quad (2)$$

respectively. We then concatenate $\tilde{X}'_{t < T/2}$ and $\tilde{X}'_{t > T/2}$, resulting in $\tilde{L} = 512$ that are used to compute $p(\hat{\mathbf{a}})$. A diagram corresponding to the token pooling and the heads workflow is depicted in Fig. 2. We ablate in §5.2 different strategies to generate the final tokens.

Training During training, the output tokens are forwarded to the corresponding heads to predict the L triplets $\hat{y}_l = \langle \hat{\mathbf{b}}_l, p(\alpha)_l, p(\hat{\mathbf{a}})_l \rangle$ with $l \in [0, L-1]$. We use the Hungarian Algorithm to match these predictions to the ground-truth instances. A ground-truth instance with N bounding boxes is defined as $y_j = \langle \mathbf{b}_j, \alpha_j = 1, \mathbf{a}_j \rangle$ for $j < N$, and as $y_j = \langle \mathbf{b}_j, \alpha_j = \emptyset, \mathbf{a}_j = \emptyset \rangle$. The matching cost between a prediction \hat{y}_i and a ground-truth triplet y_j is defined as

$$\mathcal{C}(\hat{y}_i, y_j) = \mathbb{1}_{[\alpha=1]} \mathcal{L}_{box}(\mathbf{b}_j, \hat{\mathbf{b}}_i) - \mathcal{L}_{actor}(\alpha_j, p(\alpha_i)) - \mathbb{1}_{[\alpha=1]} \mathcal{L}_{class}(\mathbf{a}_j, p(\mathbf{a}_i)) \quad (3)$$

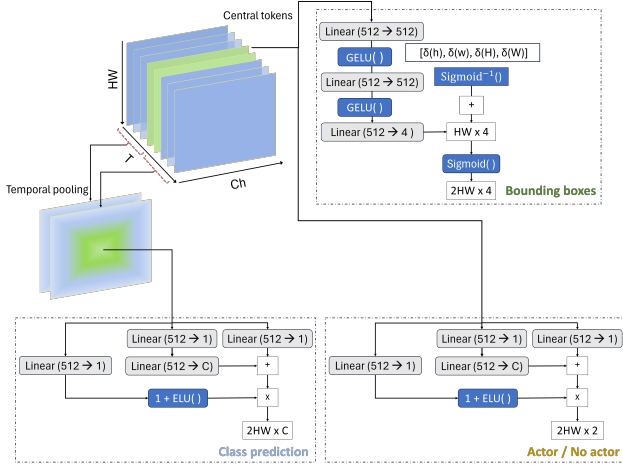


Figure 2. The output spatio-temporal tokens are fed to 3 parallel heads. We use the central tokens to predict the bounding box and the actor likelihood while averaging the output tokens over the temporal axis to generate the action tokens. Each head comprises a small MLP that generates the output triplets. We depict the flow diagram for each head, following the standard OWL-ViT head [24].

with \mathcal{L}_{box} the bounding box loss, $\mathcal{L}_{actor}(\alpha_j, p(\alpha_i)) = -\alpha_j \log p(\alpha_i)$ and $\mathcal{L}_{class}(\mathbf{a}_j, p(\mathbf{a}_i)) = -\sum_c \mathbf{a}_{i,c} \log p(\mathbf{a}_{j,c})$ (recall that \mathbf{a} is a vector of 1s and 0s representing the multi-label nature of the problem, and $p(\mathbf{a}_{j,c})$ represents the model confidence for class c). Following DETR [1] the bounding box loss is defined as $\mathcal{L}_{box}(\mathbf{b}, \hat{\mathbf{b}}) = \mathcal{L}_{iou}(\mathbf{b}, \hat{\mathbf{b}}) + \|\mathbf{b} - \hat{\mathbf{b}}\|_1$, with \mathcal{L}_{iou} the generalized IoU loss [28].

Once an optimal assignment $i = \sigma(j) \forall i \in [0, \dots, L-1]$ is found, we compute the *Hungarian Loss* as:

$$\mathcal{L} = \sum_{j=1}^L [\mathbb{1}_{[\alpha=1]} (\lambda_{iou} \mathcal{L}_{iou}(\mathbf{b}, \hat{\mathbf{b}}) + \lambda_{L1} \|\mathbf{b} - \hat{\mathbf{b}}\|_1) - \lambda_\alpha \mathcal{L}_{actor}(\alpha_j, p(\alpha_{\sigma(j)})) - \lambda_a \mathbb{1}_{[\alpha=1]} \mathcal{L}_{class}(\mathbf{a}_j, p(\mathbf{a}_{\sigma(j)}))] \quad (4)$$

where $\lambda = \{\lambda_{iou}, \lambda_{L1}, \lambda_\alpha, \lambda_a\} \in \mathbb{R}^4$ are hyperparameters.

Inference During inference, we compute the L output triplets, and we simply keep the detections of those for which $p(\alpha) > \theta$ with θ a hyperparameter that controls the trade-off between precision and recall.

4. Experimental Setup

Datasets. We use AVA 2.2 [9, 17] to conduct our main experiments and ablations, and UCF101-24 [31] and JHMDB51-21 [12] to demonstrate the generalising capabilities of our approach. AVA 2.2 [9, 17] is a long-tail dataset with 299 videos of 15-minute duration, annotated with bounding boxes and 80 action classes at 1 FPS rate. The training and validation partitions contain 235 and 64

stage	operators	output sizes
data	stride $4 \times 1 \times 1$	$16 \times 256 \times 256$
cube ₁	$3 \times 7 \times 7, 96$ stride $2 \times 4 \times 4$	$96 \times 8 \times 64 \times 64$
scale ₂	$\begin{bmatrix} \text{MHPA}(96) \\ \text{MLP}(384) \end{bmatrix} \times 1$	$96 \times 8 \times 64 \times 64$
scale ₃	$\begin{bmatrix} \text{MHPA}(192) \\ \text{MLP}(768) \end{bmatrix} \times 2$	$192 \times 8 \times 32 \times 32$
scale ₄	$\begin{bmatrix} \text{MHPA}(384) \\ \text{MLP}(1536) \end{bmatrix} \times 11$	$384 \times 8 \times 16 \times 16$
scale ₅	$\begin{bmatrix} \text{MHPA}(768) \\ \text{MLP}(3072) \end{bmatrix} \times 2$	$768 \times 8 \times 16 \times 16$
proj	$1 \times 1 \times 1, 512$	$512 \times 8 \times 256$
head	$\begin{cases} \text{MLP}(512) \\ \text{MLP}(512) \\ \text{MLP}(512) \end{cases}$	$\begin{cases} 512 \times 4 \\ 512 \times 2 \\ 512 \times C \end{cases}$

Table 1. The network architecture resembles that of MViT2-S [19], with the pooling layer after scale₄ removed. The output features are projected to 512 dimensions and forwarded to three parallel heads that predict for each token the bounding box coordinates, the probability of the bounding box being an actor, and the class predictions.

videos, amounting to 211k and 57k frames, respectively. We follow the standard evaluation protocol and report our results on the 60-class subset of annotated actions [5, 6, 25, 43]. UCF101-24 [31] contains 3207 untrimmed videos, and contains box labels and annotations on a per-frame basis, with 24 classes. We follow the standard protocol defined in [30] and report our results on split-1. JHMDB51-21 [12] has 928 trimmed videos that are labeled with 21 action categories. We follow prior work and report the average results on the three splits. For all datasets, we report the standard mean average precision (mAP) computed considering as false positives all predictions corresponding to bounding boxes with IoU < 0.5 w.r.t. a ground-truth box.

Implementation details: We initialize our model weights from the publicly available checkpoint of [19] pretrained on Kinetics-400 [14]. The network architecture and the output sizes are summarized in Tab. 1. The input to the model is $T = 16$ frames sampled at a stride of $\tau = 4$. All experiments are done using PyTorch [26]. We train our models using AdamW [23] with weight decay 0.0001, and set the trade-off hyperparameters in Eq. (4) to $\lambda_\alpha = 2.0$, $\lambda_a = 6.0$, $\lambda_{L1} = 5.0$, and $\lambda_{iou} = 2.0$. We use a batch size of 16 clips, and we train our models using 8 GeForce 3090 GPU cards. We train our model for 25 epochs with initial learning rate of 0.0001 and cosine decay with no restarts. During training, we resize the videos to 256 pixels without cropping. We add jitter to the ground-truth bounding boxes and apply color augmentation. We report our results using a single view with the input images directly resized to 256×256 pixels.

Setting ($t \times hw$)	GFLOPs	mAP
MViTv2-S [19]	64 + 246	26.8
Inp: 16×224^2 , Out: 8×7^2	65	26.8
Inp: 16×224^2 , Out: 8×14^2	87.9	27.4
Inp: 16×256^2 , Out: 8×8^2	90.7	27.5
Inp: 16×256^2 , Out: 8×16^2	121.2	30.0

(a) vs MViT + ROI align

Method	mAP	Prec.	Recall
Singleton	28.5	84.2	90.4
Tubelet	28.7	83.2	90.5
C + T	29.1	81.1	92.7
Max Pooling	28.3	84.1	91.3
2(C+T)	30.0	80.0	92.0

(b) Token Selection

Method	mAP
Variable aspect ratio	28.5
Fixed aspect ratio	30.0

(c) Impact of aspect ratio

Table 2. Ablation studies on AVA 2.2 All experiments are done using an MViTv2-S [19] pre-trained on K400. **a)** We study the relation between complexity and input/output resolutions, by removing or not the last pooling stride. Note that MViTv2-S [19] requires external bounding boxes, reportedly adding 246 GFLOPs to the overall inference. **b)** We study the impact of different methods for token selection to perform the bipartite matching. **c)** We study whether keeping the input aspect ratio affects the training, observing that a variable number of tokens results in difficult convergence.

5. Ablation studies

We perform a series of ablation studies that affect the tradeoff between complexity and accuracy, as well as on the token selection design.

5.1. vs MViT + ROI align

We first show that our method offers significant improvement w.r.t. the standard two-stage approach of MViT. Because removing the last pooling stride of our model increases the number of FLOPs, we also train a model that preserves the original MViT structure. In such a scenario, the output is a volume of $t = 8$, $h = w = 8$ for an input resolution of 256×256 . In the MViT + ROI align setting [19] a temporal pooling layer is added to remove the time dimension, and ROI align is used to extract the actor features from pre-computed bounding boxes. The actor-specific features are forwarded to a classifier to predict the class probabilities. In our setting, we generate a set of 64 triplets consisting of bounding box coordinates with their corresponding actor likelihoods and class probabilities. We keep the predictions corresponding to the tokens for which the actor likelihood is over a threshold empirically set to be $\theta = 0.2$. We also consider reducing the FLOPs by working at a lower resolution and study how our method works at a resolution of 224 pixels. The output number of tokens when working at 224 resolution reduces to 14×14 . We finally explore the scenario where the resolution is dropped to 224, and the pooling layers are left as in the original MViTv2. Such a model produces only 7×7 tokens at the central frame.

5.2. Token Selection

As mentioned in §3.4, the output of a model is a sequence of $\tilde{L} = 2048$ tokens. We reduce such number by considering the central tokens for the bounding box regression and the actor likelihood $p(\alpha)$ and the half-based temporal pooling of the spatio-temporal output tokens to consider the class probabilities. This reduction results in $\tilde{L} = 512$ tokens for the bipartite matching problem. However, other alternatives

can be explored that exploit the spatio-temporal information in a different manner. Considering that the aforementioned approach uses the central tokens and the past and future tubelets w.r.t the central frame for the actor detection and action classification, respectively, we refer to this method as **2(C + T)**. The central frame corresponds to the slice of $h \times w$ tokens at $t = \lfloor T/2 \rfloor$. We explore the alternatives below and report our results in Tab. 2b, illustrating the tradeoff between accuracy and detection precision and recall.

Singletons The simplest approach is to consider all $\tilde{L} = 2048$ tokens to predict the bounding boxes and action class probabilities.

Tubelets Our first alternative is to apply temporal pooling on the output embeddings, generating a single set of $\tilde{L} = h \times w = 256$ tokens. These tokens are then forwarded to the corresponding MLPs to compute the bounding boxes and class predictions. Such average pooling can benefit the classification task but compromise the detection performance.

C + T . This approach considers only 256 tokens. The $h \times w$ tokens corresponding to $t = \lfloor T/2 \rfloor$ are used to predict the bounding boxes and the actor likelihoods. To compute the action classes, we average over the temporal axis to form a single $h \times w$ set of output tokens.

Max pooling of class predictions In this setting, the actor tokens are computed from the central tokens. The full list of $\tilde{L} = t \times h \times w$ of output embeddings is forwarded to the classification head, producing $\tilde{L} \times C = (thw) \times C$ predictions. These can be then max-out over the temporal domain to be reduced to the necessary $\tilde{L} = (hw) = 256$ predictions.

The results in Tab. 2b indicate that a proper token selection is important to achieve a good tradeoff between detection and classification. We observe that two factors affect the most to improve the mAP: a high recall in the bounding box detection and a good selection of representatives for action tokens.

5.3. Fixed vs Variable Aspect Ratio

Often, detection frameworks apply a scale augmentation by resizing the images to different scales, and by keeping the aspect ratio in the case of transformers. Such augmentation incurs a variable number of tokens \tilde{L} to be assigned for each clip, which might affect the learning. We compare both approaches by training our model using a scale range between 240 and 340 pixels and keeping the aspect ratio. As shown in Tab. 2c, the performance drops significantly with respect to using a fixed number of tokens. We attribute this effect of matching a variable number of tokens to the ground-truth during training, which might require further hyperparameter optimization to improve convergence. We leave for future work improving the training in the case of variable-size images.

5.4. Qualitative analysis

In Fig. 5 we show a visual demonstration of how the tokens carry the actor information properly. The left images show the confidence maps (i.e. $p(\alpha)$) for each of the $h \times w$ tokens at $t = \lfloor T/2 \rfloor$ (for the sake of clarity we illustrate only the confidence maps for the frame where the actor confidences were resulting in positive detections). We can see that the tokens around the actors in the frame are more confident than those that are farther away. In the right images, we overlap all the bounding boxes computed for the same $h \times w$ tokens, representing in yellow those corresponding to the activated tokens. We can see that while there are other bounding boxes around the two actors, only those that are maximally overlapping the ground-truth activate the actor likelihood with high confidence. We include more qualitative results in the Supplementary Material.

6. Comparison with State-of-the-art

6.1. Performance on AVA 2.2

Our method is benchmarked against the current state-of-the-art approaches reported in AVA 2.2, as summarized in Tab. 3. We use symbols ✕ to denote methods relying on pre-computed bounding boxes, indicating a two-stage process, and symbols ✓ for those employing a single-stage approach. Additionally, we provide insights into the computational costs associated with each method. We note that two-stage methods listed in Tab. 3 utilize bounding boxes generated by [6], leveraging a FasterRCNN-R101-FPN network which demands 246 GFLOPs on an input resolution of 512 pixels [1]. We divide our comparison according to the methods that are pretrained on Kinetics 400 [37], and those that use external data or other self-supervision methods for pre-training.

Comparison with models pre-trained on K400: We are mostly interested in attaining increased accuracy at a low



Figure 3. Qualitative analysis. The images on the **left** show the confidence maps produced by the output 16×16 spatial tokens (rescaled to the image size) w.r.t. the actor likelihood for the corresponding bounding box. For the sake of clarity, we only plot the 256 tokens corresponding to one of the frames. The highlighted tokens are those selected as positive detections. The images on the **right** show all the bounding boxes computed by the corresponding tokens on the left. We overlay all the bounding boxes returned by each of the 16×16 output tokens. In yellow we represent the bounding boxes corresponding to the confident tokens represented on the left. All other bounding boxes (in red) are assigned to the no-class label \emptyset , and are thus considered as negative predictions

computational cost. When comparing our method to two-stage approaches, we note that our method using MViTv2-16 \times 4 as the backbone surpasses all MViT methods, and achieves higher accuracy than MeMViT, with much fewer FLOPs.

Comparison with recent single stage approaches: We are now interested in comparing our method against TubeR [43], STMixer [41] and EVAD [2] which are the latest works on single-stage action detector and all build on DETR. For a fair comparison, and given that we have trained on models initialized on Kinetics 400, we do not report and compare large models pre-trained on K700. In K400 we acquire 30.0

Method	Pretraining	mAP	GFLOPs	Res.	Backbone	End-to-end
ACAR-Net [25]	K400	28.8	205 + 246	256	SF-R50-NL	✗
MViTv1-B [5]	K400	27.3	455 + 246	224	MViTv1-B	✗
MViTv2-S [19]	K400	26.8	65 + 246	224	MViTv2-S	✗
MViTv2-B [19]	K400	28.1	225 + 246	224	MViTv2-B	✗
MeMViT [39]	K400	28.5	59 + 246	224	MViTv1	✗
WOO [3]	K400	25.4	148	256	SF-R50	✓
STMixer [41]	K400	27.8	N/A	256	SF-R50	✓
Ours	K400	30.0	121	256	MViTv2-S 16 × 4	✓
VideoMAE [35]	K400, VideoMAE	31.8	180+246	224	ViT-B	✗
VideoMAE [35]	K400, VideoMAE	37.0	597+246	224	ViT-L	✗
UMT [18]	K400, UMT	32.7	180+246	224	ViT-B	✗
UMT [18]	K400, UMT	39.0	596+246	224	ViT-L	✗
Hiera-L [29]	K400, MAE	39.8	413+246	224	Hiera-L	✗
TubeR [43]	K400, IG65M [7]	29.2	97	256	CSN-50	✓
TubeR [43]	K400, IG65M [7]	33.4	138	256	CSN-152	✓
EVAD [2]	K400, VideoMAE	32.3	243	288	ViT-B	✓
STMixer [41]	K400, VideoMAE	32.6	N/A	256	ViT-B	✓
Ours	K400, MAE	38.5	650	256	Hiera-L	✓

Table 3. Comparison to the state-of-the-art (reported with mean Average Precision; mAP ↑) on AVA v2.2 [9]. “Res.” denotes the frame resolution.

mAP comparable to TubeR and STMixer. We deem that our method, however, offers a much simpler solution without explicit context modeling and without the use of a decoder.

Scaling up to large backbones: While the scope of our proposed approach is to develop efficient methods for training a video transformer for action localization, we explore how our proposed approach scales to larger models. To this end, we train a Hiera-L [29] in an end-to-end fashion using the publicly available checkpoint pre-trained on Kinetics400, which was first pre-trained in a self-supervised manner using Masked AutoEncoders [10]. We directly reuse our training recipe to train the large model, without any further parameter optimization. In this setting, we observe that our approach competes with the two-stage approach of Hiera-L [29], although results in sub-par performance. We attribute this sub-par performance to the difficulty of training large models in an end-to-end fashion. We leave for future work and investigation the optimization of big models in our setting.

6.2. Additional Datasets

To demonstrate the effectiveness of our approach we evaluate our method on **UCF101-24** [31] and **JHMDB51-21** [12] datasets. Results of our approach are shown in Tab. 4. In UCF101-24 our method outperforms the current state-of-the-art while for JHMDB achieves comparable results. We note that compared to EVAD [2] we have similar performance with a backbone of much smaller capacity, i.e. our backbone has 121 GFLOPs while EVAD [2] has 243 GFLOPs. Our approach surpasses EVAD on UCF24, and lies behind in JHMDB. However, we observed that our model attains a precision and recall of 99% on JHMDB, indicating that further attention needs to be put towards improving accuracy.

Method	End-to-end	$T \times \tau$	Backbone	JHMDB	UCF24
CA-RCNN [40]	✗	32×2	R50-NL	79.2	-
AIA [34]	✗	32×1	R50-C2D	-	78.8
ACAR-Net [25]	✗	32×1	SF-R50	-	84.3
ACT [13]	✓	6×1	VGG	65.7	69.5
MOC [17]*	✓	7×1	DLA32	70.8	78.0
ACRN [33]	✓	20×1	S3D-G	77.9	-
YOWO [15]	✓	16×1	3D-X101	80.4	74.4
WOO [3]	✓	32×2	SF-R101-NL	80.5	-
TubeR [43]*	✓	32×2	I3D	80.7	81.3
TubeR [43]	✓	32×2	CSN-152	-	83.2
STMixer [41]	✓	32×2	SF-R101-NL	86.7	83.7
EVAD [2]	✓	16×4	ViT-B	90.2	85.1
Ours	✓	16×4	MViTv2-S	80.7	85.6

Table 4. Comparison with the state-of-the-art on UCF101-24 and JHMDB. ✓ denotes an end-to-end approach using a unified backbone, and ✗ denotes the use of two separated backbones, one of which is Faster R-CNN-R101-FPN (246 GFLOPs [27]) to pre-compute person proposals. $T \times \tau$ refers to the frame number and corresponding sample rate. Methods marked with * leverage optical flow input.

7. Conclusion

In this paper, we presented a simple method for the direct training of Vision Transformers for end-to-end action localization. We showed that the output tokens of a vision transformer can be independently forwarded to corresponding MLP heads to have a fixed sequence of predictions similar to DETR. Using a bipartite matching loss it is possible to train the backbone directly to perform both tasks without compromising performance. Our results show that simple models achieve similar accuracy to equivalent two-stage approaches.

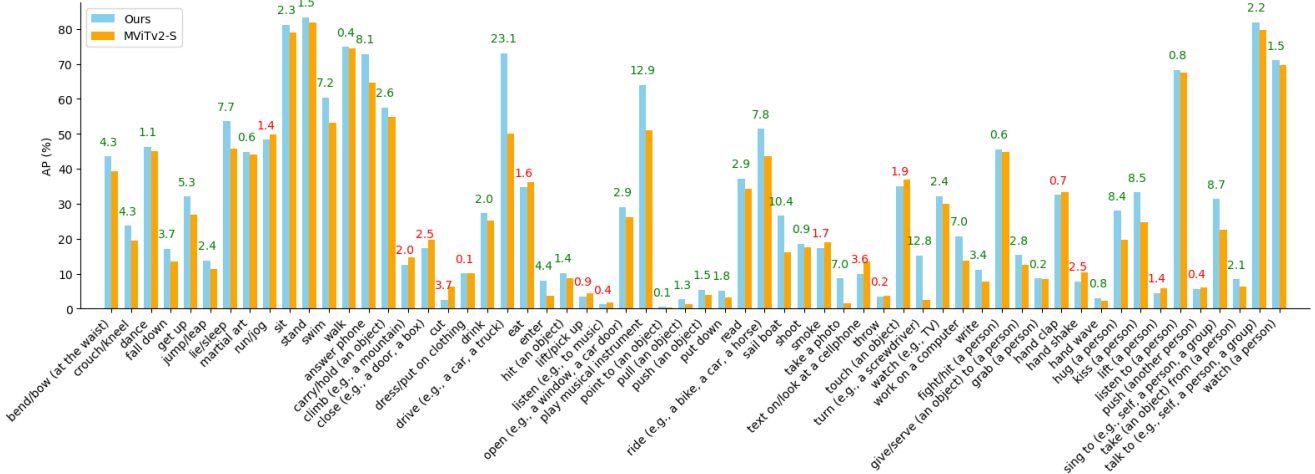


Figure 4. Per-category AP for **Ours** single stage action detection method (30.0 mAP) and **MViTv2-S** (27.0 mAP) on AVA v.2. On top of the bar there is the difference per-class where categories with increased accuracy are marked in **green** and those decreased with our method are in **red**.

A. Per-class analysis

In Fig. 4 we present the performance per-category of our single-stage model built on MViTv2-S [19] and the corresponding two-stage approach of the same MViT on AVAv2.2 [17]. To compute the per-class accuracy, we re-trained the backbone using the same settings as in [19], obtaining 27.05 mAP, which is indeed +0.2 w.r.t. the reported results. Our approach demonstrates improvements in 44 out of the 60 categories, notably increasing in categories like 'drive (e.g., a car, a truck)' with an impressive +23.1 mAP increase and 'turn (e.g., a screwdriver)' with a significant +12.8 mAP boost. Intriguingly, the performance trends across categories remain consistent between our method and the two-stage MViT, suggesting the feasibility of employing the same representation for both actor localization and action detection tasks.

B. Visual analysis

In Fig. 5 we show three visual examples complementing those presented in Fig. 3 in the main paper. In these examples, we also show the attention maps for each of the tokens that are chosen to represent an actor with $p(\alpha) > \theta$. We can see that the attention maps show how each token is indeed tracking the actor for which they carry the corresponding information, illustrating how our approach can enable the visual tokens to carry bounding box information regarding the central frame, as well as the class information that requires spatio-temporal reasoning.

References

- [1] Nicolas Carion, Francisco Massa, Gabriel Synnaeve, Nicolas Usunier, Alexander Kirillov, and Sergey Zagoruyko. End-to-end object detection with transformers. In *ECCV*, 2020. 1, 3, 5, 7
- [2] Lei Chen, Zhan Tong, Yibing Song, Gangshan Wu, and Limin Wang. Efficient video action detection with token dropout and context refinement. In *ICCV*, 2023. 2, 3, 7, 8
- [3] Shoufa Chen, Peize Sun, Enze Xie, Chongjian Ge, Jiannan Wu, Lan Ma, Jiajun Shen, and Ping Luo. Watch only once: An end-to-end video action detection framework. In *ICCV*, 2021. 2, 8
- [4] Alexey Dosovitskiy, Lucas Beyer, Alexander Kolesnikov, Dirk Weissenborn, Xiaohua Zhai, Thomas Unterthiner, Mostafa Dehghani, Matthias Minderer, Georg Heigold, Sylvain Gelly, Jakob Uszkoreit, and Neil Houlsby. An image is worth 16x16 words: Transformers for image recognition at scale. In *ICLR*, 2021. 3
- [5] Haoqi Fan, Bo Xiong, Karttikeya Mangalam, Yanghao Li, Zhicheng Yan, Jitendra Malik, and Christoph Feichtenhofer. Multiscale vision transformers. In *ICCV*, 2021. 2, 5, 8
- [6] Christoph Feichtenhofer, Haoqi Fan, Jitendra Malik, and Kaiming He. Slowfast networks for video recognition. In *ICCV*, 2019. 2, 5, 7
- [7] Deepti Ghadiyaram, Matt Feiszli, Du Tran, Heng Wang Xueting Yan, and Dhruv Mahajan. Large-scale weaklysupervised pre-training for video action recognition. In *CVPR*, 2019. 8
- [8] Rohit Girdhar, Joao Carreira, Carl Doersch, and Andrew Zisserman. Video action transformer network. In *CVPR*, 2019. 2
- [9] Chunhui Gu, Chen Sun, David A. Ross, Carl Vondrick, Caroline Pantofaru, Yeqing Li, Sudheendra Vijayanarasimhan, George Toderici, Susanna Ricco, Rahul Sukthankar, Cordelia Schmid, and Jitendra Malik. AVA: A video dataset of spatio-

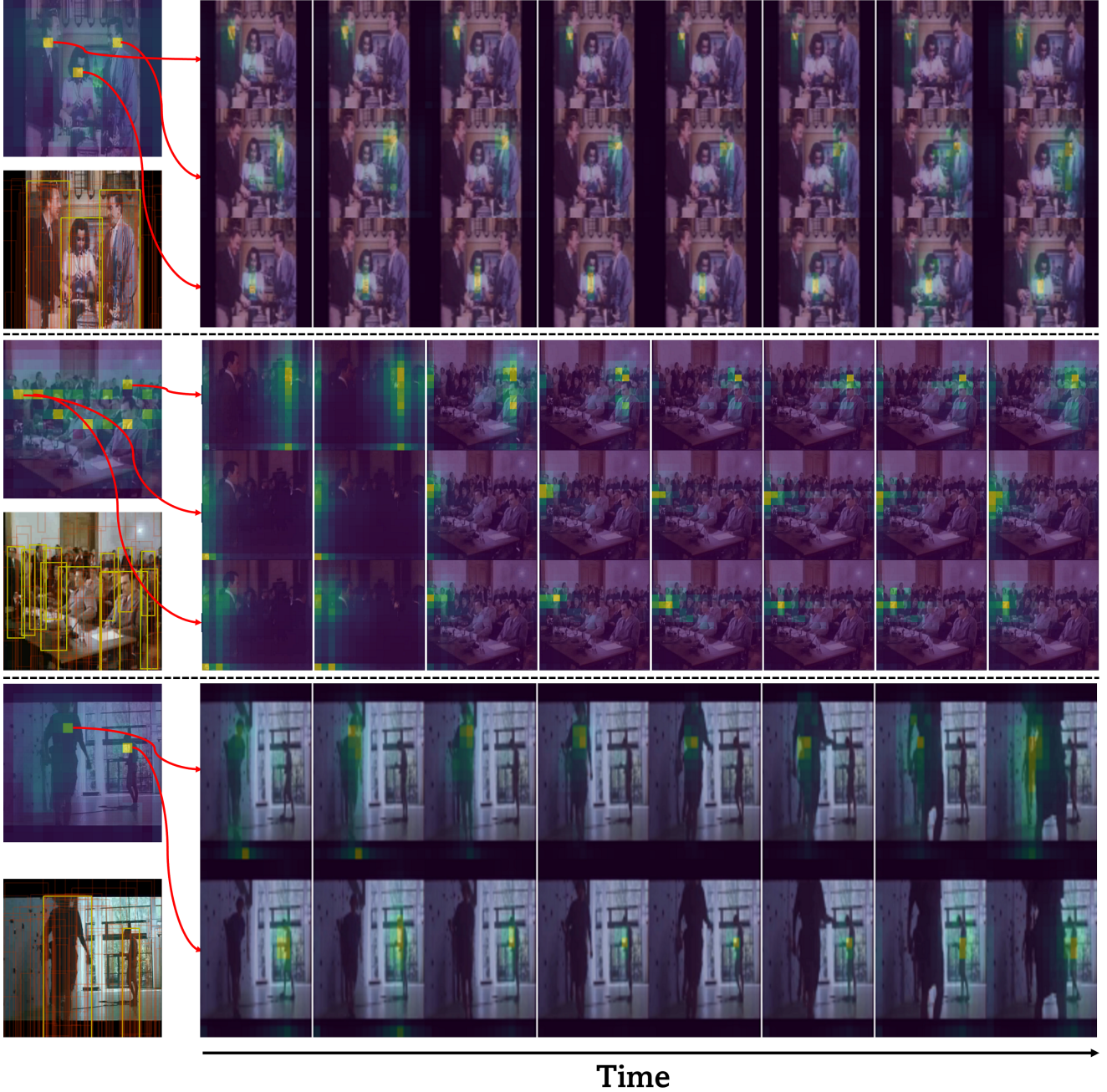


Figure 5. Qualitative analysis (better seen in color and zoomed in). We provide three qualitative examples from three corresponding validation videos from AVA2.2. On the **left top** image we represent the confidence scores $p(\alpha)$ for the actor-no actor prediction for each of the 16×16 output tokens corresponding to one of the central frames. Those with high confidence $p(\alpha) > \theta$ are selected as positive examples, and their corresponding bounding boxes and class predictions will then form the final outputs. The images in the **left bottom** are the bounding boxes predicted by each of the same 16×16 output tokens, with those in yellow corresponding to the positive tokens (i.e. to the final output bounding boxes). On the **right** we represent the last layer’s attention maps corresponding to each of the selected tokens in the left, i.e. their attention scores w.r.t. the whole $8 \times 16 \times 16$ spatio-temporal tokens. We observe that the confident tokens not only attend to the central information to produce the bounding box but also track the corresponding actor across the video to estimate the corresponding actions. In the second example, we only represent three actors for the sake of clarity. We observe that even with a change of scene, the attention maps can properly track each actor’s information. In the last example, the self-attention maps show how they can track each actor’s despite the self-occlusion. These examples show that our method can track the actor’s information and regress the bounding boxes with a Vision Transformer that assigns each vision token a different output, which are assigned to the ground-truth set through bipartite matching.

- temporally localized atomic visual actions. In *CVPR*, 2018. 2, 5, 8
- [10] Kaiming He, Xinlei Chen, Saining Xie, Yanghao Li, Piotr Dollár, and Ross Girshick. Masked autoencoders are scalable vision learners. In *CVPR*, 2021. 8
- [11] Kaiming He, Georgia Gkioxari, Piotr Dollar, and Ross Girshick. Mask r-cnn. In *ICCV*, 2017. 2, 3
- [12] Hueihan Jhuang, Juergen Gall, Silvia Zuffi, Cordelia Schmid, and Michael J Black. Towards understanding action recognition. In *ICCV*, 2013. 5, 8
- [13] Vicky Kalogeiton, Philippe Weinzaepfel, Vittorio Ferrari, and Cordelia Schmid. Action tubelet detector for spatio-temporal action localization. In *ICCV*, 2017. 8
- [14] Will Kay, Joao Carreira, Karen Simonyan, Brian Zhang, Chloe Hillier, Sudheendra Vijayanarasimhan, Fabio Viola, Tim Green, Trevor Back, Paul Natsev, et al. The kinetics human action video dataset. *arXiv preprint arXiv:1705.06950*, 2017. 5
- [15] Okan Köpüklü, Xiangyu Wei, and Gerhard Rigoll. You only watch once: A unified cnn architecture for real-time spatiotemporal action localization. In *arXiv preprint arXiv:1911.06644*, 2019. 2, 8
- [16] Harold W. Kuhn. The Hungarian Method for the Assignment Problem. *Naval Research Logistics Quarterly*, 2(1–2):83–97, March 1955. 3
- [17] Ang Li, Meghana Thotakuri, David A Ross, João Carreira, Alexander Votrikov, and Andrew Zisserman. The avakinetis localized human actions video dataset. *arXiv preprint arXiv:2005.00214*, 2020. 1, 2, 5, 8, 9
- [18] Kunchang Li, Yali Wang, Yizhuo Li, Yi Wang, Yinan He, Limin Wang, and Yu Qiao. Unmasked teacher: Towards training-efficient video foundation models. In *ICCV*, 2023. 8
- [19] Yanghao Li, Chao-Yuan Wu, Haoqi Fan, Karttikeya Mangalam, Bo Xiong, Jitendra Malik, and Christoph Feichtenhofer. MViTv2: Improved multiscale vision transformers for classification and detection. 2022. 2, 3, 5, 6, 8, 9
- [20] Tsung-Yi Lin, Michael Maire, Serge J. Belongie, Lubomir D. Bourdev, Ross B. Girshick, James Hays, Pietro Perona, Deva Ramanan, Piotr Dollár, and C. Lawrence Zitnick. Microsoft COCO: common objects in context. 2014. 2
- [21] Tsung-Yi Lin, Piotr Dollár, Ross Girshick, Kaiming He, Bharath Hariharan, and Serge Belongie. Feature pyramid networks for object detection. In *CVPR*, 2017. 3
- [22] Tsung-Yi Lin, Michael Maire, Serge Belongie, James Hays, Pietro Perona, Deva Ramanan, Piotr Dollár, and C Lawrence Zitnick. Microsoft coco: Common objects in context. In *ECCV*, 2014. 1
- [23] Ilya Loshchilov and Frank Hutter. Decoupled weight decay regularization. *arXiv preprint arXiv:1711.05101*, 2017. 5
- [24] Matthias Minderer, Alexey Gritsenko, Austin Stone, Maxim Neumann, Dirk Weissenborn, Alexey Dosovitskiy, Aravindh Mahendran, Anurag Arnab, Mostafa Dehghani, Zhuoran Shen, Xiao Wang, Xiaohua Zhai, Thomas Kipf, and Neil Houlsby. Simple open-vocabulary object detection with vision transformers. In *ECCV*, 2022. 1, 4, 5
- [25] Junting Pan, Siyu Chen, Mike Zheng Shou, Yu Liu, Jing Shao, and Hongsheng Li. Actor-context-actor relation network for spatio-temporal action localization. In *CVPR*, 2021. 2, 5, 8
- [26] Adam Paszke, Sam Gross, Francisco Massa, Adam Lerer, James Bradbury, Gregory Chanan, Trevor Killeen, Zeming Lin, Natalia Gimelshein, Luca Antiga, et al. Pytorch: An imperative style, high-performance deep learning library. *Advances on Neural Information Processing Systems*, 2019. 5
- [27] Shaoqing Ren, Kaiming He, Ross Girshick, and Jian Sun. Faster r-cnn: Towards real-time object detection with region proposal networks. *Advances in neural information processing systems*, 2015. 1, 2, 8
- [28] Hamid Rezaatofghi, Nathan Tsoi, JunYoung Gwak, Amir Sadeghian, Ian Reid, and Silvio Savarese. Generalized intersection over union: A metric and a loss for bounding box regression. In *CVPR*, 2019. 5
- [29] Chaitanya Ryali, Yuan-Ting Hu, Daniel Bolya, Chen Wei, Haoqi Fan, Po-Yao Huang, Vaibhav Aggarwal, Arkabandhu Chowdhury, Omid Poursaeed, Judy Hoffman, Jitendra Malik, Yanghao Li, and Christoph Feichtenhofer. Hiera: A hierarchical vision transformer without the bells-and-whistles, 2023. 2, 8
- [30] Gurkirt Singh, Suman Saha, Michael Sapienza, Philip HS Torr, and Fabio Cuzzolin. Online real-time multiple spatiotemporal action localisation and prediction. In *ICCV*, 2017. 5
- [31] Khurram Soomro, Amir Roshan Zamir, and Mubarak Shah. Ucf101: A dataset of 101 human actions classes from videos in the wild. *arXiv preprint arXiv:1212.0402*, 2012. 5, 8
- [32] Lin Sui, Chen-Lin Zhang, Lixin Gu, and Feng Han. A simple and efficient pipeline to build an end-to-end spatial-temporal action detector. In *WACV*, 2022. 2
- [33] Chen Sun, Abhinav Shrivastava, Carl Vondrick, Kevin Murphy, Rahul Sukthankar, and Cordelia Schmid. Actor-centric relation network. In *ECCV*, 2018. 2, 8
- [34] Jiajun Tang, Jin Xia, Xinzhi Mu, Bo Pang, and Cewu Lu. Asynchronous interaction aggregation for action detection. In *ECCV*, 2020. 2, 8
- [35] Zhan Tong, Yibing Song, Jue Wang, and Limin Wang. VideoMAE: Masked autoencoders are data-efficient learners for self-supervised video pre-training. In *Advances on Neural Information Processing Systems*, 2022. 2, 8
- [36] Oytun Ulutan, Swati Rallapalli, Carlos Torres, Mudhakar Srivatsa, and B Manjunath. Actor conditioned attention maps for video action detection. In *IEEE Winter Conference on Applications of Computer Vision*, 2020. 2
- [37] Philippe Weinzaepfel, Zaid Harchaoui, and Cordelia Schmid. The kinetics human action video dataset. 2017. 7
- [38] Chao-Yuan Wu, Christoph Feichtenhofer, Haoqi Fan, Kaiming He, Philipp Krahenbuhl, and Ross Girshick. Long-term feature banks for detailed video understanding. In *CVPR*, 2019. 2
- [39] Chao-Yuan Wu, Yanghao Li, Karttikeya Mangalam, Haoqi Fan, Bo Xiong, Jitendra Malik, and Christoph Feichtenhofer. Memvit: Memory-augmented multiscale vision transformer for efficient long-term video recognition. In *CVPR*, 2022. 2, 8
- [40] Jianchao Wu, Zhanghui Kuang, Limin Wang, Wayne Zhang, and Gangshan Wu. Context-aware RCNN: A baseline for action detection in videos. In *ECCV*, 2020. 2, 8

- [41] Tao Wu, Mengqi Cao, Ziteng Gao, Gangshan Wu, and Limin Wang. Stmixer: A one-stage sparse action detector. In *CVPR*, 2023. 1, 2, 3, 7, 8
- [42] Yubo Zhang, Pavel Tokmakov, Martial Hebert, and Cordelia Schmid. A structured model for action detection. In *CVPR*, 2019. 2
- [43] Jiaojiao Zhao, Xinyu Li, Chunhui Liu, Shuai Bing, Hao Chen, Cees GM Snoek, and Joseph Tighe. Tuber: Tube-transformer for action detection. *arXiv preprint arXiv:2104.00969*, 2021. 1, 2, 3, 5, 7, 8